A microfluidic electrochemical cell with integrated PdH reference electrode for high current experiments

Espen V. Fanavoll[a,b], David A. Harrington[b], Svein Sunde[a], Gurvinder Singh[a], Frode Seland[a,*]

[a] *Department of Materials Science and Engineering, NTNU, Norwegian University of Science and Technology, N-7491 Trondheim, Norway*
[b] *Department of Chemistry, University of Victoria, Victoria, BC, V8W 3V6 Canada*

Abstract

An on-chip thin-film palladium hydride reference electrode is described for use with microfluidic electrochemical cells. A Pd electrode fabricated by photolithographic methods is charged with hydrogen in-situ with a simple current step technique. The placement of the reference electrode in a side channel means that it is unaffected by species in the main channel. Placement upstream of the working and sense electrodes is shown to be a significant improvement over cells with the reference electrode placed externally. The adverse effects of solution resistance are investigated quantitatively, and it is shown that the described configuration allows for high current experiments while maintaining accurate potential measurement. A simple formula for calculating the maximum current density for a certain cell geometry and electrolyte resistivity is presented.

Keywords: Microfluidics, Electrochemistry, Palladium hydride, Reference electrodes, IR drop

1. Introduction

Microfluidic devices have the potential to be a valuable addition to the electrochemistry toolbox. Key advantages include highly controllable and well described convective mass transport conditions, the ability to work with electrolyte volumes below 1 mL, and the ability to rapidly switch the electrolyte using microchannels with multiple inlets. The cells can be designed to include several downstream electrodes for detection of soluble reaction products and intermediates. Microfluidic cells can be rapidly prototyped using photolithography and metal evaporation techniques, supporting cell designs with micron-level precision, and multiple electrodes of different composition. Deposition of catalyst particles on the microelectrodes is also possible, enabling the study of electrocatalytic reactions in these kinds of cells.

Applications of electrochemical microfluidic devices include biosensors [1–4], membraneless fuel cells [5–9], velocimetry [10, 11], electrosynthesis [12–14], water treatment [15, 16], fuel reformers [17], CO_2 conversion [18] and investigation of electrocatalysts [19].

Electrochemical experiments require a reference electrode to reliably measure electrode potentials. Using a reference electrode in a three-electrode setup allows for the study of processes at the working electrode without the influence of the reaction at the counter electrode [e.g. 20]. Traditional reference electrodes, such as the saturated calomel electrode, the Ag/AgCl electrode [19, 21, 22] or the hydrogen reference electrode, are very large compared to the cell, and need to be placed in an external chamber, typically downstream of the electrodes in the channel. It is important that the counter electrode is situated downstream of the working electrode to avoid the processes taking place there influencing the concentration of species at the working electrode. This configuration is the source of an inaccuracy in the measurement of working electrode potentials due to uncompensated solution resistance. Moreover, external reference electrodes negate some of the attractive features of a fully integrated lab-on-chip device.

Integrated pseudo reference electrodes [23] based on gold [24, 25] or Ag/AgCl [26–30] have been used in lab-on-chip devices, but reporting potential measurements against these electrodes is problematic, as they are not based on thermodynamic equilibrium [31], or they are not separated from the sample electrolyte. Some successful implementations of stable integrated Ag/AgCl reference electrodes have been made, using laminar flow [32] or a nanochannel [33] in order to separate the sample electrolyte from the reference electrolyte while maintaining electrical contact. When working with platinum or gold electrodes however, it is advisable to avoid the presence of chloride ions due to adsorption and anodic corrosion of the electrode [34–36]. A certain constant amount of Cl^- ions is necessary to maintain a thermodynamically stable reference potential, and concentrations down to 10 ppm [37] can be harmful, especially to nanoparticle catalysts. Thomas et al. [38] demonstrated several thin film metal/metal ion refer-

*Corresponding author
Email addresses: espen.v.fanavoll@ntnu.no (Espen V. Fanavoll), dharr@uvic.ca (David A. Harrington), svein.sunde@ntnu.no (Svein Sunde), gurvinder.singh@ntnu.no (Gurvinder Singh), frode.seland@ntnu.no (Frode Seland)

ence electrodes with non-electroactive anions. Integrated reference electrodes can also be based on a reversible redox couple in solution [10, 39] such as $Ru(NH_3)_6^{2+/3+}$ or $Fe(CN)_6^{3-/4-}$, but these will both be affected by, and affect the measurement of other species in the solution. A more extensive review of the most common microfabricated reference electrodes can be found in Shinwari et al. [40].

One of the experimental challenges with performing electrochemical measurements in microfluidic cells, and the topic of this paper, is the effect of solution resistance caused by the restricted volume of the microchannel. This can create large potential gradients in the microchannel when a current flows, which imposes severe limitations to the currents that can be applied to electrodes in the microchannel without losing accuracy in the measured electrode potentials. The main focus of electrochemical microfluidics has been low-current or single electrode sensing applications [1, 41–43], where the potential distribution, or even the electrode potential itself, is subordinate. Currents up to tens of nanoamperes typically cause potential shifts of less than a millivolt [19] in a microchannel. For a typical experimental setup, using a 1 mm x 50 µm channel and 0.1 M sulfuric acid as the electrolyte, the channel resistance per unit length becomes $43\,\mathrm{k\Omega\,cm^{-1}}$ at 20 °C (data from [44]). This is manageable for currents up to tens of nanoamperes, but for currents on the scale of microamperes, which is relevant for many electrochemical reactions, the potential distribution and reference electrode placement must be considered in order to report accurate electrode potentials. Knowledge and control of the potential distribution also gives a higher degree of flexibility in cell design and choice of supporting electrolytes.

In standard electrochemical cells the reference electrode is placed as close in the potential field to the working electrode as possible, for instance using a Luggin capillary, in order to minimize the uncompensated solution resistance R_s [45]. In a microfluidic cell with an external reference electrode, R_s becomes the full resistance between the working and counter electrodes, instead of just a fraction of it. Significant shifts in the potential sensed by the reference electrode can occur when current flows between the working and counter electrodes.

Problems with uncompensated solution resistance are compounded when working with multiple electrodes in the same microchannel, for instance using a downstream sense electrode to detect the products of the working electrode. The current through one of the electrodes will influence the solution potential above the other electrodes. This influence has been described for microchannels with external reference electrodes [21, 46, 47] at various electrode distances, and must be accounted for to be able to report accurate potential measurements.

The internal palladium hydride reference electrode is a possible alternative to using traditional reference electrodes. Palladium can incorporate large amounts of hydrogen as a palladium hydride alloy, with an α-phase at mole fractions up to 0.017, and a mix of α and β (or α') phase up to a fraction of 0.58 at room temperature [48].

Palladium hydride electrodes generated from palladium wire have been found to hold a stable potential at 50 mV against a hydrogen reference electrode at the same pH [49]. This potential is generally attributed to the α-β phase transition of the PdH alloy [50]. As this reference electrode only requires a palladium metal electrode which can be charged in situ, it is relatively simple to fabricate by the same photolithographic method as the rest of the microfluidic cell, and it can easily be integrated in the cell upstream of the working electrode. One of the main concerns with the PdH reference electrode is the period of stable potential, as the alloy loses hydrogen to the electrolyte.

Imokawa et al. [51] reported fabrication and application of nanostructured PdH microelectrodes with lifetimes of 1-3 hours in deaerated solutions. Webster and Goluch [4] reported a microfabricated PdH reference electrode in a nanochannel, that was stable for up to 1 hour. In both these cases, an external reference electrode was used to load the Pd structure with hydrogen.

In this work we present a microfluidic electrochemical cell with an internal palladium hydride reference electrode placed in a side channel upstream of the working electrode. This configuration proves to be a significant improvement over cells with external reference electrodes, allowing for higher-current electrochemical experiments to be performed in the microchannel. The reference electrode design has the advantages over previous PdH electrodes that it is not in the working fluid, it can be charged without an external reference electrode, and it is stable for at least 5 hours.

2. Experimental

2.1. Device fabrication

The fabrication of microfluidic flow cells was performed by photolithography and metal evaporation techniques at the NorFab NanoLab cleanroom facilities at NTNU. A lift-off lithography process was performed twice to produce electrodes of platinum and palladium on the same glass slide. The detailed fabrication recipe is provided in the supplementary information.

The cells were assembled from a glass slide with the electrodes and a PDMS slab with a 1 mm wide and 90 µm high microchannel. Device assembly is relatively simple and does not require extreme precision in aligning the PDMS slab on top of the electrode assembly. The electrodes were deposited by electron beam evaporation, with a thickness of 190 nm on top of a 10 nm Ti adhesion layer. The electrode slide includes a palladium reference electrode (REF), platinum working (WE) and counter electrodes (CE), and a platinum sense electrode (SE) with varying distance to the working electrode. Figure 1 shows

the cell design, along with an image of a fully assembled cell and a microscope image of electrodes of the same cell. The edge-to-edge distance between the working and sense electrodes are defined as d. Four different cells were used, with the WE-SE gaps 100, 300, 500 and 700 µm. The typical distance from the working electrode to the internal reference electrode is 5 mm and the distance to the outlet chamber is approximately 10 mm, as can be seen from figure 1a, though this can vary slightly with the alignment of the channel slab.

2.2. Electrochemical measurements

Electrochemical experiments were performed in a 50 mM phosphate buffer electrolyte (H_3PO_4 and Na_2HPO_4), with 0.1 M Na_2SO_4 supporting electrolyte (all Sigma Aldrich). The buffer solution was calculated and measured to be pH 3.0. Half-wave potentials were recorded in 1 mM tris(2,2-bipyridyl)dichlororuthenium(II) hexahydrate (Sigma Aldrich) in the buffer electrolyte, the electroactive species being $Ru(bpy)_3^{2+}$. Electrolyte solutions were purged with Ar gas for at least 20 minutes before being filled into the syringe.

Assembled cells were dried and stored in a glovebox (<4 ppm O_2) for at least a day before use, in order to remove oxygen from the PDMS. The cells were then kept in a plastic box under N_2 gas during the experiment. Glass syringes with PTFE plungers (1000 LT, Hamilton) were used when the electrolyte had to be kept oxygen free, e.g. for the reference channel inlet, otherwise disposable plastic syringes (HSW GMBH) were used.

A syringe pump (Pump 11 Pico Plus Elite, Harvard Apparatus) was used to control electrolyte flow through the main channel inlet. The reference side channel was kept stagnant during measurement, and regularly flushed with clean electrolyte. Electrochemical measurements were performed using a Biologic VMP3 potentiostat, with two channels connected to common counter and reference electrodes.

The PdH reference electrode (REF) was charged at a constant current of −5 µA (−0.5 mA cm^{-2}) for at least 5 minutes, then left to stabilize at open circuit for at least 30 minutes. All potentials in this paper are quoted versus this internal reference electrode, unless otherwise specified.

For measurements against an external reference electrode, a reversible hydrogen electrode was placed in an external chamber at the electrolyte outlet, in the same electrolyte as the rest of the system.

After the reference stabilization period, the Pt electrodes were cycled at between 0 and 1.5 V at 500 mV s^{-1} in the buffer electrolyte for at least 30 cycles or until the voltammograms were stable, in order to clean the electrode.

The potential distribution in the microchannel was probed by measuring the half-wave potential $E_{1/2}$ of the oxidation of $Ru(bpy)_3^{2+}$ at constant flow rate, at the SE, while a current step technique was performed at the WE. Both

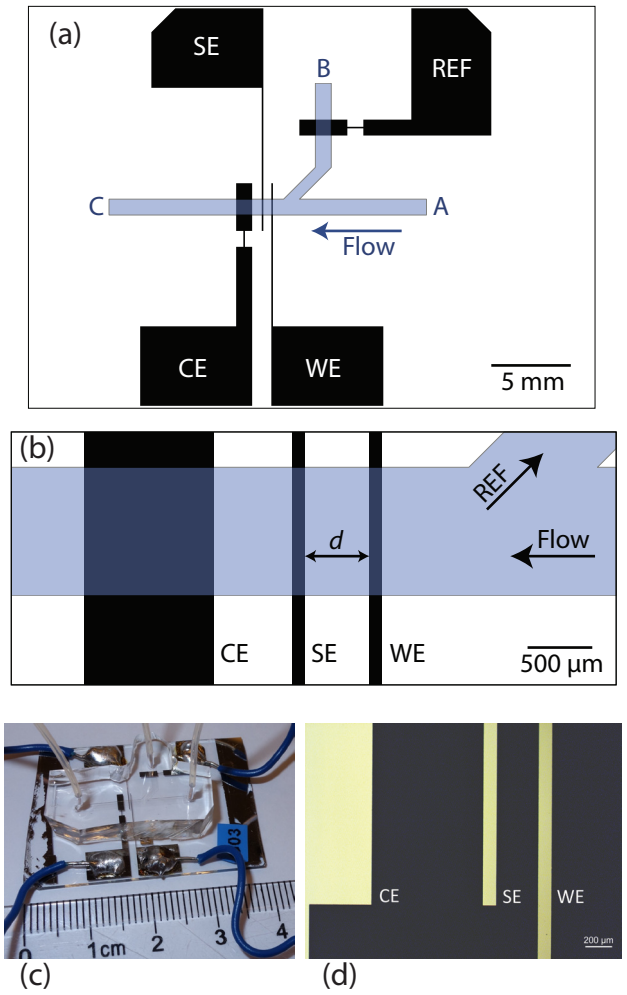

Figure 1: Microfluidic cell. (a) Top-down view of an electrode slide, drawn to scale. The reference electrode (REF) is a 1 mm wide Pd electrode, the working (WE) and sense (SE) electrodes are 100 µm wide Pt electrodes, and the counter electrode (CE) is a 1 mm wide Pt electrode. A, B and C indicates the locations of the main electrolyte inlet, reference electrolyte inlet and electrolyte outlet, respectively. (b) Closer view of the electrodes in the main channel. d is defined as the edge-to-edge distance between WE and SE. (c) Picture of assembled cell. (d) Microscope image of electrodes in main channel.

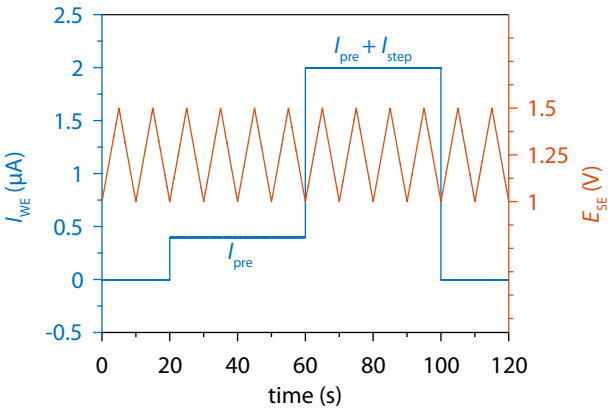

Figure 2: Applied waveforms. Blue: Chronopotentiometry steps applied to the WE. Red: Voltammetry cycles applied to the SE. The current on the WE was first stepped from open circuit to I_{pre} at 20 s, then stepped by a magnitude of I_{step} at 60 s. The half-wave potential shift at the SE was measured from the forward scans of the cycles directly before and after the step at 20 s.

the WE and SE was cycled at $100\,\mathrm{mV\,s^{-1}}$ between 1.0 and 1.5 V to stabilize platinum oxide on the surface. The mass transport limited current for the oxidation of $Ru(bpy)_3{}^{2+}$, I_{lim}, for the appropriate flow rate, was estimated from the maximum current when the potential cycling at the WE gave stable voltammograms. The half-wave potential shift was measured by cycling the SE at $100\,\mathrm{mV\,s^{-1}}$ from 1.0 to 1.5 V for 12 cycles, while current steps were applied to the WE. These techniques were linked so that the current steps on the working electrode were synchronized with the lower vertex points of the potential cycles on the SE, see figure 2. The SE was cycled several times per current step on the WE: first two initial cycles at open circuit, then four at a conditioning current I_{pre}, four at high current $(I_{\mathrm{pre}} + I_{\mathrm{step}})$, then two cycles at open circuit at the end. The magnitude of the step from the conditioning current to high current is defined as I_{step}. This was repeated for increasing values of I_{step}, up to 100 µA. The conditioning current I_{pre} was chosen to be slightly higher than the estimated limiting current, in order to ensure that the concentration ratio $c_{Ru(bpy)_3{}^{2+}}/c_{Ru(bpy)_3{}^{3+}}$ was constant over the high-current step. The half wave potentials were measured from the cycles directly before and after the high-current step, and the other cycles were used to validate the experiment, as the measurement was only considered valid if the voltammograms for each step were stable for all the cycles.

3. Results and discussion

3.1. The internal PdH reference electrode

The internal PdH reference electrode was generated in-situ from the Pd thin film electrode at the start of the experiment. As the electrode is charged at a constant current, no external reference electrode is required, and the process can even be monitored using a downstream electrode to measure hydrogen gas, as is discussed below. The reference electrode can be generated with or without flow, though it is recommended to occasionally flush the channel to remove trapped hydrogen gas. Measurements of the PdH electrode potentials during and after charging were performed using an external reversible hydrogen reference electrode (RHE) in the same electrolyte.

The potential of the PdH electrode was found to drift during the first 30 minutes after charging, before reaching a stable potential. When measured against the RHE, the stable potential of the thin-film PdH reference electrode was $(75 \pm 5)\,\mathrm{mV}$. Figure 3b shows the continuous measurement of the electrode potential, with a stable period of 5 hours in a thoroughly deaerated cell.

In cells with no external reference, the PdH reference electrode was stable for up to 8 hours after charging, as inferred from hydrogen adsorption and desorption potentials at platinum. This PdH stability is difficult to demonstrate directly in cells with an external reference owing to practical complications in connection with the latter.

The potential of the reference electrode drifted by 1-$2\,\mathrm{mV\,h^{-1}}$ over the operation period. The stability of the reference electrode was found to be very sensitive to the concentration of dissolved oxygen in the reference electrolyte. With the cell outside of the nitrogen-purged box, the PdH reference discharged within 15 minutes. For a moderately deaerated cell, i.e. a cell kept in an N_2-atmosphere for ∼4 hours, the potential typically remained stable for 2 hours.

Figure 3a shows the charging potential of a PdH electrode, with potentials measured against a reversible hydrogen electrode placed in a chamber at the electrolyte outlet. The potential during charging goes through two plateaux, most clearly seen in the logarithmic plot. The first lasts 10 s, and corresponds to the formation of the α phase (low H solubility), and the second corresponds to the formation of the β phase (high H solubility).

Visually, the palladium-hydrogen alloy had a darker tint than the parts of the electrode not exposed to electrolyte. The electrode returned to its normal color after being depleted of hydrogen during the experiments, and no visible changes or damage to the electrode were observed even after multiple charging cycles. As long as the faradaic processes at the palladium electrode were controlled, the reusability of the reference electrode was excellent. One palladium electrode was charged and discharged 15 times without measurable damage.

Figure 4 shows the measurement of the open circuit potential at the WE vs. RHE performed simultaneously with the charging of the PdH reference electrode in figure 3a. The platinum electrode acts as a hydrogen sensor downstream of the charging reference electrode, with the potential moving towards 0 vs. the RHE as the amount of hydrogen gas in the electrolyte increases. At a flow rate of $20\,\mathrm{\mu L\,min^{-1}}$, transport time from the RHE to the WE is around 1.6 s. Note that the steps in the potential at 0 and

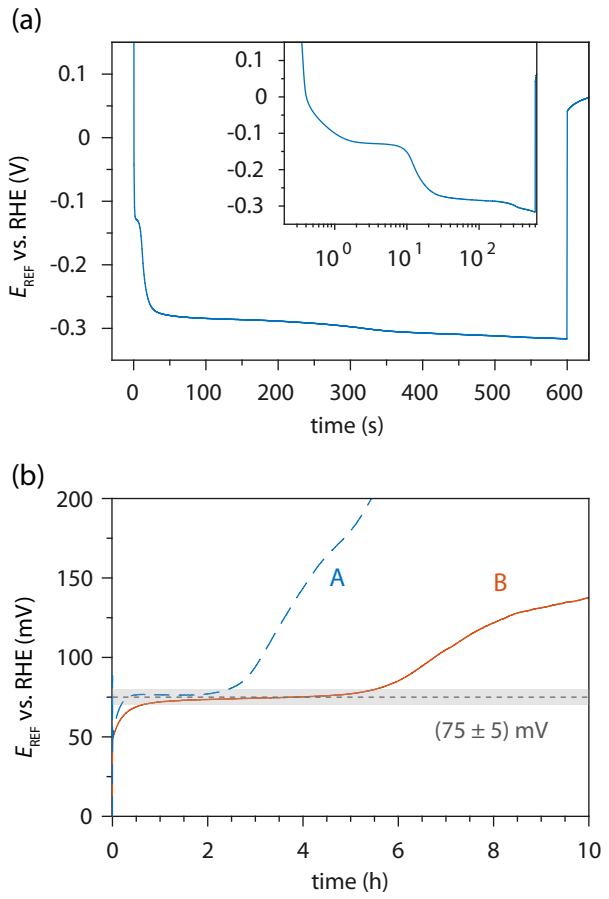

Figure 3: PdH reference electrode charging and discharging transients. a) Charging a 1 mm wide thin-film Pd electrode (REF). Constant current at $-5\,\mu A$ from $t = 0$ to $t = 600\,s$. Flow rate $20\,\mu L\,min^{-1}$ through the reference side channel. Potential measured against a RHE in an outlet chamber. Inset shows the time on a log scale. b) Open circuit potentials of the PdH reference electrode directly after charging, in a moderately (A) and thoroughly (B) deaerated cell.

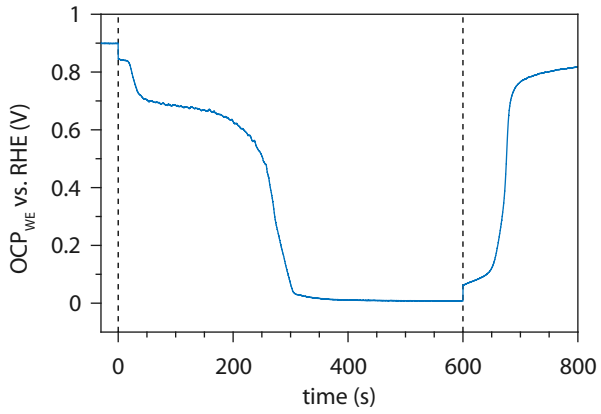

Figure 4: Downstream detection of hydrogen during PdH reference electrode charging. Measurement of the open circuit potential at WE vs. an external RHE during charging of the PdH reference electrode at a flow rate of $20\,\mu L\,min^{-1}$ (figure 3) The potential flattens sharply at 300 s.

600 s are due to IR drop between REF and CE when current flows between the electrodes. The potential decreases after 20 s, showing that not all of the hydrogen produced at the reference electrode is absorbed into the palladium. The open circuit potential decreases more rapidly after 200 s and flattens sharply at 300 s. This indicates that the release of hydrogen into the electrolyte at the reference electrode is near constant between 300 and 600 s.

The charge passed during 300 s at $-5\,\mu A$ is 1.5 mC, surpassing the calculated theoretical charge of 1.2 mC required to reach the pure β-phase in the exposed part of the Pd electrode. Based on this, we assume that the exposed part of the thin-film electrode is mostly converted to β phase PdH alloy during the charging. Whether more hydrogen is absorbed into the alloy beyond this point can not be discerned from this experiment. No adverse effects of charging the reference for longer than 300 s were observed in practice, and the time required for potential stabilization was similar whether the charging was aborted at 300 s or continued to 600 s. Charging for shorter times led to shorter or absent stable potential periods.

One drawback with the thin-film PdH reference electrode was an increased pickup of electromagnetic noise compared to an external reference electrode. This was solved by operating the cell in a grounded Faraday cage.

The PdH reference electrode is reliable as long as certain precautions are taken. Firstly, the potential of the electrode will drift by about $1\,mV\,h^{-1}$as the PdH β phase is depleted of hydrogen, and up to $5\,mV\,h^{-1}$ towards the end of the lifetime. This must be taken into account when reporting potentials against this reference. If possible, a known potential should be used to verify the reference potential and check the drift, for instance before and after the measurement. This could be towards an external reference electrode, a known electrochemical couple, or the hydrogen adsorption peaks of a clean Pt electrode.

Secondly, the pH of the reference electrolyte should be constant. During longer experiments it is possible that the species in the main electrolyte channel diffuse into the reference channel, even if it is kept stagnant. It is advisable to use the same electrolyte, or at least have the same pH in the main and reference electrolyte.

Third and finally, the absence of oxygen is very important to the stability of the reference. Electrolytes must be purged with inert gas before measurements, and it is advisable to use glass syringes to keep the electrolyte deaerated during the experiments. PDMS is oxygen permeable, so the cell should be kept under inert atmosphere before and during the experiment. A short exposure to air when transferring the cell from storage to the experimental setup did not seem to have a measurable effect, but having the cell exposed to air for longer periods eventually introduced oxygen into the electrolyte.

Compared to other integrated reference electrodes for microfluidic cells, the main advantage of this reference electrode is the simplicity of the cell design and operation. The lifetime of a single charge is long enough for many

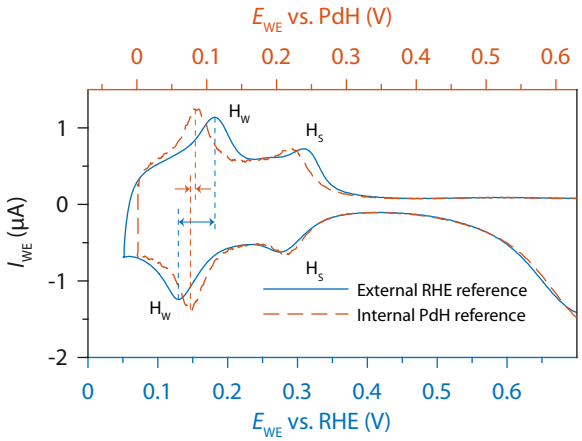

Figure 5: Strong (H_S) and weak (H_W) hydrogen adsorption and desorption peaks of a 100 µm platinum electrode (WE), recorded by cyclic voltammetry at 500 mV s^{-1} against an external RHE reference electrode (blue, solid, bottom axis) and against the internal PdH reference electrode (red, dotted, top axis). The separation of the weak adsorption/desorption peaks (H_W) with the external reference electrode is 53 mV, and 7 mV with the internal PdH reference electrode.

continuous electrochemical experiments, and the ability to recharge the reference electrode in-situ sets it apart from other electrodes. The stability of integrated Ag/AgCl reference electrodes varies with the complexity of the design and fabrication. Simple electrodes of similar dimensions fabricated by thin film methods show similar or lower stability than this one [40]. This is due to the limited amount of Ag and AgCl making the electrode vulnerable to dissolution. Higher stability has been achieved by employing additional fabrication steps such as electroplating [26] to increase the amount of available silver, or coating the electrode with a polymer [28] or KCl-gel [30] to inhibit dissolution. In any case, an ion-conductive barrier would be required to avoid contamination of the working electrolyte, as the Ag/AgCl electrode is typically operated in Cl^- concentrations above 0.1 M. The non-contaminating reference electrolyte for the PdH electrode allows for a simpler cell design.

3.2. The effect of solution resistance and reference electrode placement on a single electrode in a microchannel

With a fully functional integrated reference electrode, the effects of reference electrode placement and potential distribution on the measurement of electrode potentials in the microchannel can be investigated. This section describes the effects on a single electrode, comparing the integrated (upstream) reference electrode with an external (downstream) one.

The peak separation of strong hydrogen adsorption and desorption peaks was analyzed by cyclic voltammetry at 500 mV s^{-1} (Figure 5), first using an external reversible hydrogen electrode placed in an outlet chamber, and then with the internal PdH reference electrode. The peak separation was 53 mV when using the external reference electrode, and 7 mV when using the internal one.

These hydrogen adsorption and desorption peaks are characteristic features of platinum voltammograms. Ideally, there should be no peak separation [45]. The peak separation observed here is due to uncompensated solution resistance. This shows that even when performing electrochemical measurements on a single electrode, the effects of solution resistance and reference electrode placement in a microchannel can be significant.

These adsorption and desorption currents are small compared to the currents for the electrocatalytic reactions typically studied using these electrodes, and higher currents lead to larger potential shifts. This clearly shows that the configuration with the internal reference electrode is better suited for higher current experiments.

3.3. The effect of solution resistance on multiple electrodes in a microchannel

When working with multiple electrodes in a microchannel, the situation becomes more complicated, as the currents at one electrode may influence the solution potentials at other electrodes in the channel. By moving the reference electrode upstream of the WE this is simplified, as the current on the SE should not influence the potential at the WE in this configuration. The current applied to the WE, however, will influence the potential at the SE or any additional electrodes downstream, and the magnitude of this influence will be quantified in this section. Figure 6 illustrates the expected potential distribution in the channel with currents flowing through the electrodes. This is derived from a simple equivalent electrical circuit for the microfluidic cell, where electrode width is not considered. An anodic current through the WE, with CE as the counter electrode, is expected to shift the solution potential Φ_{sol} above the SE to lower potentials with a magnitude of $I_{WE} \times R_s$.

The shift in the solution potential above the SE was measured using the half-wave potential $E_{1/2}$ of the oxidation reaction of $Ru(bpy)_3^{2+}$, while oxygen was produced at the WE upstream. This redox system was chosen due to its stability, fast charge transfer, and that the redox potential can be fixed between the potentials for oxygen evolution and reduction on Pt by choosing the right pH. The voltammograms for this system at the flow rates used in this section are shown in figure 7a.

At any potential where H_2O is oxidized, the WE will also oxidize $Ru(bpy)_3^{2+}$, so it was necessary to take both oxidation reactions into consideration when performing the current step. To account for this, the half wave potential was measured at the SE, first with the WE at a conditioning current (I_{pre}) slightly above the mass transport limited current of $Ru(bpy)_3^{2+}$, then again at a higher current with significant oxygen evolution. This ensures that the ratio of $c_{Ru(bpy)_3^{2+}}/c_{Ru(bpy)_3^{3+}}$ in the Nernst equation

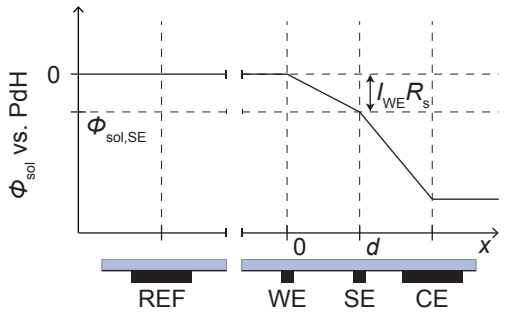

Figure 6: Expected potential distribution in the microchannel when an anodic current flows through both the WE and the SE, with CE as the common counter electrode. Derived from simple equivalent circuit of the cell. The current flowing between the WE and REF is negligible, so there is no potential gradient between these electrodes in the simplified case.

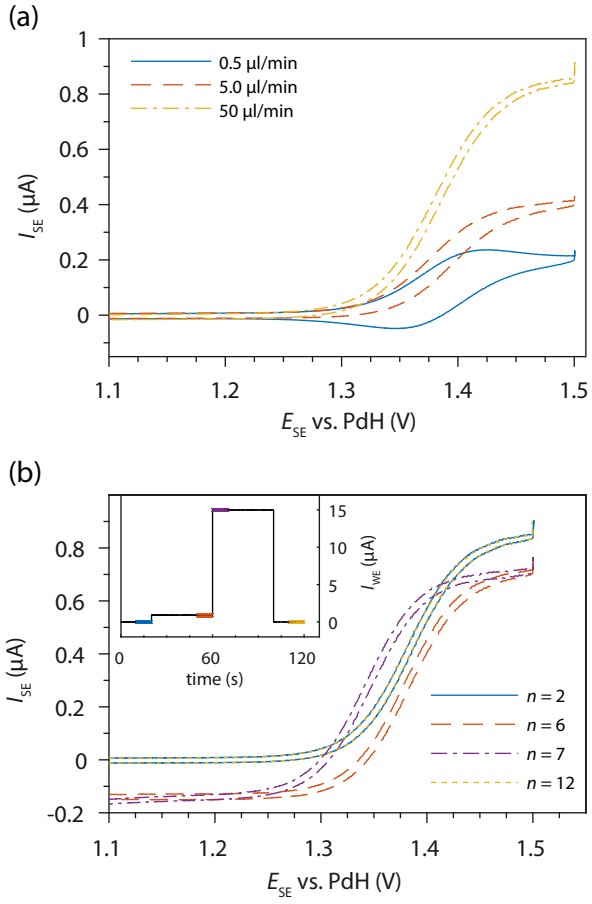

Figure 7: Voltammetry of the $Ru(bpy)_3^{2+}$ redox system. (a) Typical voltammograms recorded at 100 mV s^{-1} at the different flow rates used in this work. (b) Cyclic voltammetry at the SE at different parts of the current steps on the WE (n is the cycle number); n=2 and n=12 are with WE at open circuit (and overlap completely), n=6 and n=7 are with the WE at the conditioning and high current steps. The half-wave potential shift is measured from the 6th and 7th cycles. The inset illustrates the current at the WE at the different cycles at the SE. The flow rate is 50 µL min^{-1} and the electrode gap d is 300 µm.

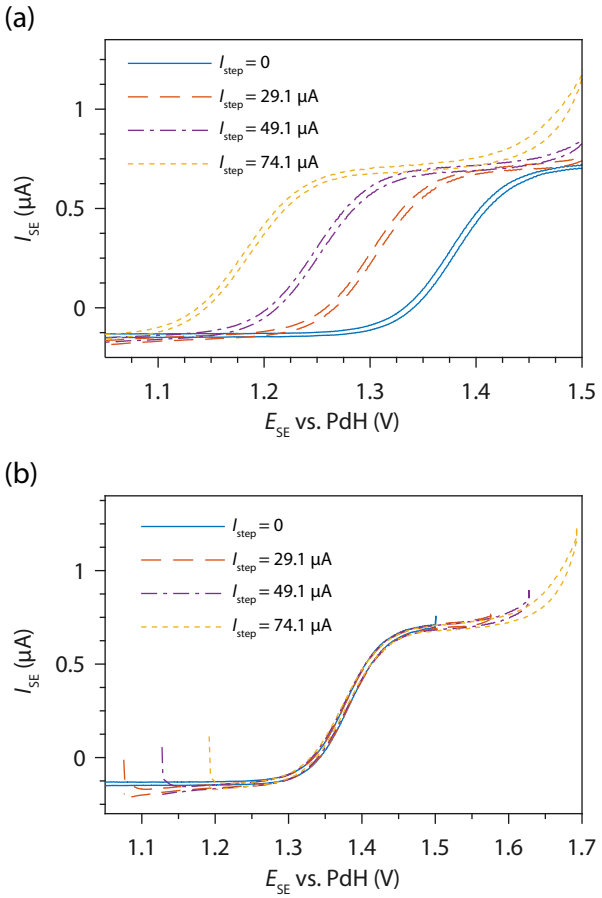

Figure 8: (a) Voltammograms recorded at the SE, cycle 6 and 7, before (I_{step} = 0) and after galvanic step on WE. Electrode gap 300 µm, flow rate 50 µL min^{-1}. (b) The same voltammograms corrected for the measured potential shift.

(1) will be constant over the current step, consequently the only difference between the voltammogram before and after the current step is the shift in solution potential Φ_{sol}.

$$E = E^\circ - \frac{RT}{F} \ln \frac{c_{red}}{c_{ox}} \quad (1)$$

Figure 7b shows the response in the voltammogram at the SE to the different chronoamperometry steps at the WE, and confirms that the method used is suitable for probing the solution potential. For n = 2 and n = 12, corresponding to I_{WE} = 0 before and after the experiment, there is complete overlap. The step from open circuit to diffusion limited current shifts the current of the voltammogram cathodically. The step from I_{pre} to higher current shifts the voltammogram to lower potentials, as is expected for anodic currents through the WE. The total current during the high-current step is $I_{pre} + I_{step}$. The experiment was repeated for a range of current steps, at flow rates of 0.5, 5 and 50 µL min^{-1}. Only the results recorded at 50 µL min^{-1} were used in the calculations, as the applicable oxygen evolution current was limited at lower flow rates due to accumulation of oxygen gas in the channel.

Figure 8a shows voltammograms for a cell with an electrode gap of 300 µm, with oxygen evolution currents of up to 74.1 µA at the WE. The potential is shifted up to 200 mV. Figure 8b shows the same voltammograms corrected by the measured half-wave potential shift. The forward scans overlap closely, verifying that the potential shift is the only difference between the voltammograms.

Figure 8b also shows a cathodic current at potentials below 1.2 V, corresponding to the reduction of oxygen gas produced at the WE. This current increases along with I_{step}, and was especially prominent at lower flow rates. When performing the same experiment in 0.1 M sulfuric acid, the potential ranges for reduction of O_2 and oxidation of $Ru(bpy)_3{}^{2+}$ overlap making measurement of the half-wave potential shift impossible. In the pH 3 buffer solution, the processes that depend on the proton concentration, including the oxygen evolution as well as the PdH reference, are shifted to lower potentials so they don't overlap with $Ru(bpy)_3{}^{2+}$ oxidation.

Figures 9a and b show the half-wave potential shifts measured for increasing I_{step} for all flow rates, and for 50 µL min^{-1} only. Figure 9c shows the data for all 4 cells, at 50 µL min^{-1}. The dashed lines are linear fits calculated by a robust (bisquare) linear least squares method. The bisquare method weights the data points closest to the fit heavier than the outliers. The slope of this line is R_{s} in $\Delta\Phi_{\mathrm{sol}} = \Delta E_{1/2} = I_{\mathrm{WE}} \times R_{\mathrm{s}}$.

Most of the data points follow the linear fit closely, though a few measurements deviate to a larger shift than expected. This is due to oxygen bubbles of significant sizes beginning to form and block parts of the channel, effectively increasing the solution resistance. At high anodic currents the oxygen evolution is significant enough to form visible gas bubbles in the channel and in the outlet tubing. This is exaggerated at higher electrode spacing and lower flow rates, and sets an upper limit to the I_{step} in this experiments. This gradual resistance increase could be seen by comparing the subsequent CV cycles after the current step, as the voltammogram continued to shift further to lower potentials even while I_{step} remained constant. Consequently, the potential shift was only taken into consideration if it was stable over the 4 cycles. The channel was periodically flushed with short bursts at high flow rate to remove residual oxygen bubbles from the channel.

In figure 9d R_{s}, as found from the slopes in figure 9c, is plotted against the electrode spacing d. Only 50 µL min^{-1} data was used in the calculation, though the lower flow rates fit the same calculations at low I_{step}-values. The dashed line is an unbound linear fit calculated by a weighted LLS method, using the inverse of the 95% confidence interval from the calculation of the R_{s} values, as the weights. This fit intersects the d-axis at $d = -93$ µm. A more appropriate definition of the electrode spacing would seem to be the center-to-center distance, rather than the edge-to-edge distance of the electrodes.

The experimental electrolyte conductivity can be calculated from the slope of the linear fit in figure 9d and the dimensions of the microchannel:

$$6.6\,\Omega\,\mu\mathrm{m}^{-1} \times 1\,\mathrm{mm} \times 90\,\mu\mathrm{m} = 0.60\,\Omega\,\mathrm{m} \rightarrow 17\,\mathrm{mS\,cm}^{-1} \quad (2)$$

The literature conductivity of 0.1 M Na_2SO_4 is 15.0 mS cm^{-1} [44]. There is also a small contribution to the conductivity from the buffer species.

While the electrode separation is very accurate in the lithography process, the channel height has been found to be not completely uniform. Variations of 5 µm in channel height are common for the SU8 channel master. This may contribute to uncertainties in predicting the solution resistance from the electrode distance and electrolyte resistivity alone, as this is dependent on the channel cross-section. The method used in this work is a more reliable method to measure the solution resistance directly.

To confirm that the potential at the WE is completely independent on the processes on the downstream electrodes, the roles of the electrodes were switched, using a cell with $d = 100$ µm. The half-wave potential of the oxidation of $Ru(bpy)_3{}^{2+}$ was measured by cyclic voltammetry, while current steps up to -50 µA was applied to the SE. As expected, this had no effect on the potential of the reaction at the WE.

3.4. When can the effects of potential distribution in the microchannel be neglected?

From the results above, it is possible to set some limits to how large the currents at the upstream electrode can be before the shifts in the solution potential at downstream electrodes have to be considered. A potential shift tolerance ΔE_{max} is defined as a limit below which the potential shift is considered to be negligible for the experiment. The corresponding maximum current I_{max} at the WE then becomes:

$$I_{\mathrm{max}} = \frac{\Delta E_{\mathrm{max}}}{R_{\mathrm{s}}} = \frac{\Delta E_{\mathrm{max}} \times w_{\mathrm{ch}} \times h_{\mathrm{ch}}}{\rho \times d_{\mathrm{c}}} \quad (3)$$

or in terms of current density:

$$j_{\mathrm{max}} = \frac{I_{\mathrm{max}}}{w_{\mathrm{ch}} \times w_{\mathrm{el}}} = \frac{\Delta E_{\mathrm{max}} \times h_{\mathrm{ch}}}{\rho \times d_{\mathrm{c}} \times w_{\mathrm{el}}} \quad (4)$$

where:

w_{ch} = channel width
h_{ch} = channel height
ρ = electrolyte resistivity
d_{c} = electrode center-to center distance
w_{el} = working electrode width

The cell used in this work with the highest value of I_{max} is the one with electrode separation $d = 100$ µm (i.e. $d_{\mathrm{c}} = 200$ µm). Equations 3 and 4 give a maximum current

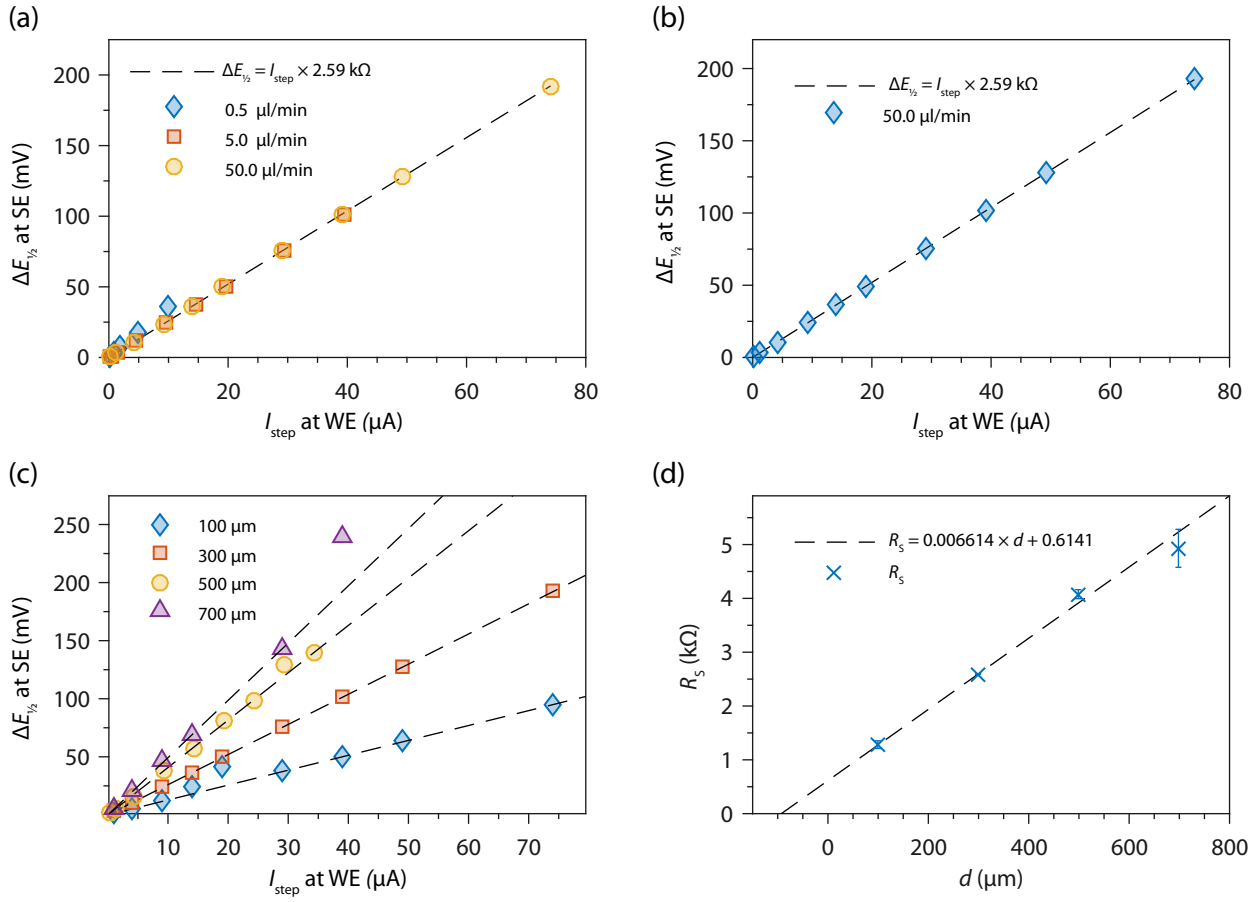

Figure 9: Measured shifts in the half-wave potential at different I_{step} currents. For the cell with electrode gap $d = 300\,\mu\text{m}$: (a) All flow rates and (b) $50\,\mu\text{L}\,\text{min}^{-1}$. (c) Potential shifts for all electrode gaps at $50\,\mu\text{L}\,\text{min}^{-1}$. (d) the slopes of the linear fits plotted against the electrode spacing, including the 95% confidence intervals. The dotted line is a weighted LLS using 1/95% confidence interval weighting. The linear fit intersects the d-axis at $d = 93\,\mu\text{m}$.

of 3.78 µA, or a current density of $3.78\,\text{mA}\,\text{cm}^{-2}$. For currents higher than this, potential shifts at the SE will be higher than the tolerance of 5 mV.

There are several possible methods for increasing the current density limit in electrochemical experiments. The simplest is to decrease the electrolyte resistivity by increasing the supporting electrolyte concentration. A second option is to modify the cell design, using smaller electrodes and further decreasing the electrode gaps. It should be possible to produce features down to 10 µm reliably by the lithography process used here.

4. Conclusion

A microfluidic cell is described with an integrated PdH reference electrode placed in a side channel upstream of the working, sense and counter electrodes situated in the main channel. The major advantage with this type of cell is that it allows for higher currents to pass through electrodes in the microchannel, while maintaining the accuracy of the measured electrode potentials. The side channel allows the reference electrode to be unaffected by the species in the main channel. In this configuration, the solution potential at one electrode is not affected by currents applied to downstream electrodes. The solution potential is affected by currents at any upstream electrodes, but this relationship is quantifiable, and it is possible to find current limits, below which this effect is negligible. This configuration is a significant improvement for electrochemical microfluidic cells, as it allows for measurements of higher currents with less inaccuracy due to potential distribution, enabling the study of electrocatalytic reactions in microfluidic cells.

For example, current densities up to $4\,\text{mA}\,\text{cm}^{-2}$ were possible without the potential at the downstream electrode changing by more than 5 mV. It is possible to increase this by an order of magnitude using a more concentrated supporting electrolyte, or a smaller electrode.

The PdH reference electrode was generated in situ by producing hydrogen at a 190 nm thick Pd thin-film electrode, creating a palladium-hydrogen alloy which was able to sustain a reference potential of $(75 \pm 5)\,\text{mV}$, measured against a reversible hydrogen electrode, for at least 5 hours, with a potential drift of around $1\,\text{mV}\,\text{h}^{-1}$. The electrode can be charged in a highly reproducible manner, with-

out the need for an external reference electrode. The reusability of the microfluidic cells was found to be excellent, with at least 15 charge-discharge cycles possible without significant damaging effects to the thin-film electrode.

Acknowledgments

This work is supported by funds from the Research Council of Norway (221899) and the Natural Sciences and Engineering Research Council of Canada (37035). The Research Council of Norway is further acknowledged for the support to the Norwegian Micro- and Nano-Fabrication Facility, NORFAB (197411). NorFab NTNU NanoLab is acknowledged for facilitating the fabrication of the microfluidic cells.

Supplementary information

Supplementary information is available online.

References

[1] D. G. Rackus, M. H. Shamsi, A. R. Wheeler, Electrochemistry, biosensors and microfluidics: a convergence of fields, Chem. Soc. Rev. 44 (2015) 5320–5340, doi:10.1039/C4CS00369A.

[2] J. Wang, Electrochemical detection for microscale analytical systems: a review, Talanta 56 (2) (2002) 223 – 231, ISSN 0039-9140, doi:http://dx.doi.org/10.1016/S0039-9140(01)00592-6.

[3] J. Khandurina, A. Guttman, Bioanalysis in microfluidic devices, Journal of Chromatography A 943 (2) (2002) 159 – 183, ISSN 0021-9673, doi:http://dx.doi.org/10.1016/S0021-9673(01)01451-0.

[4] T. A. Webster, E. D. Goluch, Electrochemical detection of pyocyanin in nanochannels with integrated palladium hydride reference electrodes, Lab Chip 12 (2012) 5195–5201, doi:10.1039/C2LC40650K.

[5] E. Kjeang, N. Djilali, D. Sinton, Microfluidic fuel cells: A review, Journal of Power Sources 186 (2) (2009) 353 – 369, ISSN 0378-7753, doi:http://dx.doi.org/10.1016/j.jpowsour.2008.10.011.

[6] E. Kjeang, R. Michel, D. A. Harrington, N. Djilali, D. Sinton, A Microfluidic Fuel Cell with Flow-Through Porous Electrodes, Journal of the American Chemical Society 130 (12) (2008) 4000–4006, doi:10.1021/ja078248c.

[7] E. Kjeang, J. McKechnie, D. Sinton, N. Djilali, Planar and three-dimensional microfluidic fuel cell architectures based on graphite rod electrodes, Journal of Power Sources 168 (2) (2007) 379 – 390, ISSN 0378-7753, doi:http://dx.doi.org/10.1016/j.jpowsour.2007.02.087.

[8] R. S. Jayashree, L. Gancs, E. R. Choban, A. Primak, D. Natarajan, L. J. Markoski, P. J. A. Kenis, Air-Breathing Laminar Flow-Based Microfluidic Fuel Cell, Journal of the American Chemical Society 127 (48) (2005) 16758–16759, doi:10.1021/ja054599k.

[9] E. R. Choban, L. J. Markoski, A. Wieckowski, P. J. Kenis, Microfluidic fuel cell based on laminar flow, Journal of Power Sources 128 (1) (2004) 54 – 60, ISSN 0378-7753, doi:http://dx.doi.org/10.1016/j.jpowsour.2003.11.052.

[10] E. Kjeang, B. Roesch, J. McKechnie, D. A. Harrington, N. Djilali, D. Sinton, Integrated electrochemical velocimetry for microfluidic devices, Microfluid Nanofluidics 3 (4) (2006) 403–416, ISSN 1613-4990, doi:10.1007/s10404-006-0128-1.

[11] C. Amatore, M. Belotti, Y. Chen, E. Roy, C. Sella, L. Thouin, Using electrochemical coupling between parallel microbands for in situ monitoring of flow rates in microfluidic channels, Journal of Electroanalytical Chemistry 573 (2) (2004) 333 – 343, ISSN 1572-6657, doi:http://dx.doi.org/10.1016/j.jelechem.2004.07.020.

[12] P. Watts, S. J. Haswell, Microfluidic combinatorial chemistry, Current Opinion in Chemical Biology 7 (3) (2003) 380 – 387, ISSN 1367-5931, doi:http://dx.doi.org/10.1016/S1367-5931(03)00050-4.

[13] S. M. MacDonald, J. D. Watkins, S. D. Bull, I. R. Davies, Y. Gu, K. Yunus, A. C. Fisher, P. C. B. Page, Y. Chan, C. Elliott, F. Marken, Two-phase flow electrosynthesis: Comparing N-octyl-2-pyrrolidoneaqueous and acetonitrileaqueous three-phase boundary reactions, Journal of Physical Organic Chemistry 22 (1) (2009) 52–58, ISSN 1099-1395, doi:10.1002/poc.1424.

[14] P. He, P. Watts, F. Marken, S. J. Haswell, Self-Supported and Clean One-Step Cathodic Coupling of Activated Olefins with Benzyl Bromide Derivatives in a Micro Flow Reactor, Angewandte Chemie International Edition 45 (25) (2006) 4146–4149, ISSN 1521-3773, doi:10.1002/anie.200600951.

[15] O. Scialdone, C. Guarisco, A. Galia, G. Filardo, G. Silvestri, C. Amatore, C. Sella, L. Thouin, Anodic abatement of organic pollutants in water in micro reactors, Journal of Electroanalytical Chemistry 638 (2) (2010) 293 – 296, ISSN 1572-6657, doi:http://dx.doi.org/10.1016/j.jelechem.2009.10.031.

[16] O. Scialdone, A. Galia, S. Sabatino, Electro-generation of H_2O_2 and abatement of organic pollutant in water by an electro-Fenton process in a microfluidic reactor, Electrochemistry Communications 26 (2013) 45 – 47, ISSN 1388-2481, doi:http://dx.doi.org/10.1016/j.elecom.2012.10.006.

[17] J. D. Holladay, E. O. Jones, M. Phelps, J. Hu, Microfuel processor for use in a miniature power supply, Journal of Power Sources 108 (12) (2002) 21 – 27, ISSN 0378-7753, doi:http://dx.doi.org/10.1016/S0378-7753(01)01011-4.

[18] D. T. Whipple, E. C. Finke, P. J. A. Kenis, Microfluidic Reactor for the Electrochemical Reduction of Carbon Dioxide: The Effect of pH, Electrochemical and Solid-State Letters 13 (9) (2010) B109–B111, doi:10.1149/1.3456590.

[19] I. Dumitrescu, D. F. Yancey, R. M. Crooks, Dual-electrode microfluidic cell for characterizing electrocatalysts, Lab Chip 12 (2012) 986–993, doi:10.1039/C2LC21181E.

[20] C. H. Hamann, A. Hamnett, W. Vielstich, Electrochemistry, Wiley, ISBN 978-3-527-31069-2, doi:10.1021/ed039pA134, 2007.

[21] N. M. Contento, P. W. Bohn, Electric field effects on current–voltage relationships in microfluidic channels presenting multiple working electrodes in the weak-coupling limit, Microfluid Nanofluidics 18 (1) (2014) 131–140, ISSN 1613-4990, doi:10.1007/s10404-014-1424-9.

[22] E. Bitziou, M. E. Snowden, M. B. Joseph, S. J. Leigh, J. A. Covington, J. V. Macpherson, P. R. Unwin, Dual electrode micro-channel flow cell for redox titrations: Kinetics and analysis of homogeneous ascorbic acid oxidation, J. Electroanal. Chem. 692 (2013) 72 – 79, ISSN 1572-6657, doi:10.1016/j.jelechem.2012.12.014.

[23] C. Bonnaud, I. Billard, N. Papaiconomou, E. Chainet, J. C. Lepretre, Rationale for the implementation of reference electrodes in ionic liquids, Phys. Chem. Chem. Phys. 18 (2016) 8148–8157, doi:10.1039/C5CP07652H.

[24] N. M. Contento, S. P. Branagan, P. W. Bohn, Electrolysis in nanochannels for in situ reagent generation in confined geometries, Lab Chip 11 (2011) 3634–3641, doi:10.1039/C1LC20570F.

[25] H. Yang, S. K. Kang, C. A. Choi, H. Kim, D.-H. Shin, Y. S. Kim, Y. T. Kim, An iridium oxide reference electrode for use in microfabricated biosensors and biochips, Lab Chip 4 (2004) 42–46, doi:10.1039/B309899K.

[26] B. J. Polk, A. Stelzenmuller, G. Mijares, W. MacCrehan, M. Gaitan, Ag/AgCl microelectrodes with improved stability for microfluidics, Sens. Actuators B 114 (1) (2006) 239 – 247, ISSN 0925-4005, doi:10.1016/j.snb.2005.03.121.

[27] J. Schnitker, D. Afanasenkau, B. Wolfrum, A. Offenhusser,

Planar reference electrodes on multielectrode arrays for electrochemical measurements of ionic currents, Phys. Statis Solidi A 210 (5) (2013) 892–897, ISSN 1862-6319, doi: 10.1002/pssa.201200850.

[28] T. Matsumoto, A. Ohashi, N. Ito, Development of a microplanar Ag/AgCl quasi-reference electrode with long-term stability for an amperometric glucose sensor, Anal. Chim. Acta 462 (2) (2002) 253 – 259, ISSN 0003-2670, doi:10.1016/S0003-2670(02)00334-3.

[29] A. Yakushenko, D. Mayer, J. Buitenhuis, A. Offenhausser, B. Wolfrum, Electrochemical artifacts originating from nanoparticle contamination by Ag/AgCl quasi-reference electrodes, Lab Chip 14 (2014) 602–607, doi:10.1039/C3LC51029H.

[30] I.-Y. Huang, R.-S. Huang, Fabrication and characterization of a new planar solid-state reference electrode for {ISFET} sensors, Thin Solid Films 406 (12) (2002) 255 – 261, ISSN 0040-6090, doi:http://dx.doi.org/10.1016/S0040-6090(01)01783-7.

[31] G. Inzelt, Handbook of Reference Electrodes, chap. Pseudo-reference Electrodes, Springer, Berlin, Heidelberg, ISBN 978-3-642-36188-3, 331–332, doi:10.1007/978-3-642-36188-3, 2013.

[32] E. V. Dydek, M. V. Petersen, D. G. Nocera, K. F. Jensen, Electrode Placement and Fluid Flow Rates in Microfluidic Electrochemical Devices, J. Electrochem. Soc. 159 (11) (2012) H853–H856, doi:10.1149/2.007211jes.

[33] J. Zhou, K. Ren, Y. Zheng, J. Su, Y. Zhao, D. Ryan, H. Wu, Fabrication of a microfluidic Ag/AgCl reference electrode and its application for portable and disposable electrochemical microchips, Electrophoresis 31 (18) (2010) 3083–3089, ISSN 1522-2683, doi:10.1002/elps.201000113.

[34] J. S. Mayell, S. H. Langer, Effect of dilute chloride ion on platinum electrodes, J. Electroanal. Chem. 7 (4) (1964) 288 – 296, ISSN 0368-1874, doi:10.1016/0022-0728(64)80102-9.

[35] J. Bittles, E. Littauer, Anodic corrosion and passivation of Pt in Cl- solutions, Corros. Sci. 10 (1) (1970) 29 – 41, ISSN 0010-938X, doi:10.1016/S0010-938X(70)80095-6.

[36] E. Iannone, Labs on Chip: Principles, Design and Technology, CRC Press, ISBN 978-1-4665-6073-4, 2014.

[37] A. B. Ofstad, M. S. Thomassen, J. L. Gomez de la Fuente, F. Seland, S. Mller-Holst, S. Sunde, Assessment of Platinum Dissolution from a Pt/C Fuel Cell Catalyst: An Electrochemical Quartz Crystal Microbalance Study, J. Electrochem. Soc. 157 (5) (2010) B621–B627, doi:10.1149/1.3327890.

[38] H. Thomas, R. Heide, A. Terfort, Thin film reference electrodes for aqueous and organic media, Sens. Actuators B 171172 (2012) 155 – 164, ISSN 0925-4005, doi: http://dx.doi.org/10.1016/j.snb.2012.02.071.

[39] T. Holm, M. Ingdal, E. V. Fanavoll, S. Sunde, F. Seland, D. A. Harrington, Mass-transport impedance at channel electrodes: accurate and approximate solutions, Electrochim. Acta 202 (2016) 84 – 89, ISSN 0013-4686, doi: 10.1016/j.electacta.2016.03.096.

[40] M. W. Shinwari, D. Zhitomirsky, I. A. Deen, P. R. Selvaganapathy, M. J. Deen, D. Landheer, Microfabricated Reference Electrodes and their Biosensing Applications, Sensors 10 (3) (2010) 1679, ISSN 1424-8220, doi:10.3390/s100301679.

[41] L. Nyholm, Electrochemical techniques for lab-on-a-chip applications, Analyst 130 (2005) 599–605, doi:10.1039/B415004J.

[42] M. Pumera, A. Merkoi, S. Alegret, New materials for electrochemical sensing VII. Microfluidic chip platforms, TrAC-Trend Anal. Chem. 25 (3) (2006) 219 – 235, ISSN 0165-9936, doi: 10.1016/j.trac.2005.08.005.

[43] R. S. Martin, P. D. Root, D. M. Spence, Microfluidic technologies as platforms for performing quantitative cellular analyses in an in vitro environment, Analyst 131 (2006) 1197–1206, doi: 10.1039/B611041J.

[44] W. M. Haynes (Ed.), CRC Handbook of Chemistry and Physics, 97th Edition (Internet Version 2017), chap. Electrical Conductivity of Aqueous Solutions, CRC Press/Taylor and Francis, Boca Raton, FL, URL `http://www.hbcpnetbase.com/`, 2016.

[45] D. Pletcher, R. Greff, R. Peat, L. Peter, J. Robinson, Instrumental Methods in Electrochemistry, chap. 6, 11, Woodhead Publishing, ISBN 978-1-898563-80-8, 206, 368, 2011.

[46] S. P. Forry, J. R. Murray, M. L. A. V. Heien, L. E. Locascio, , R. M. Wightman, Probing Electric Fields Inside Microfluidic Channels during Electroosmotic Flow with Fast-Scan Cyclic Voltammetry, Anal. Chem. 76 (17) (2004) 4945–4950, doi:10.1021/ac049591s.

[47] A. Bîrzu, J. Coleman, I. Z. Kiss, Highly disparate activity regions due to non-uniform potential distribution in microfluidic devices: Simulations and experiments, J. Electroanal. Chem. 726 (2014) 27 – 35, ISSN 1572-6657, doi: 10.1016/j.jelechem.2014.05.002.

[48] F. D. Manchester, A. San-Martin, J. M. Pitre, The H-Pd (hydrogen-palladium) System, J. Phase Equilib. 15 (1) (1994) 62–83, ISSN 1054-9714, doi:10.1007/BF02667685.

[49] A. Bard, R. Parsons, J. Jordan, Standard Potentials in Aqueous Solution, Monographs in Electroanalytical Chemistry and Electrochemistr, Taylor & Francis, ISBN 9780824772918, 1985.

[50] D. J. G. Ives, G. J. Janz, Reference electrodes, theory and practice., Academic Press, doi:10.1021/ed039pA134, 1961.

[51] T. Imokawa, K.-J. Williams, , G. Denuault, Fabrication and Characterization of Nanostructured Pd Hydride pH Microelectrodes, Anal. Chem. 78 (1) (2006) 265–271, doi: 10.1021/ac051328j.